Structural, Magnetochemical and Electrochemical Studies of Dinuclear Complexes Containing the $[V^{V}O]_2$, $[V^{IV}O]_2$, Cr^{III}_2, Mn^{III}_2 and Fe^{III}_2 Cores of a Potentially Pentadentate Phenol-Containing Ligand with (O,N,O,N,O)-Donor Atoms

Soumen Mukherjee,[a] Thomas Weyhermüller,[a] Eberhard Bothe,[a] and Phalguni Chaudhuri*[a]

Keywords: N,O ligands / Transition metals / Magnetic properties / Radicals / Electrochemistry

Dinuclear complexes $[L_2Fe^{III}_2]$ (**1**), $[L_2Mn^{III}_2]$ (**2a**), $[L_2Mn^{III}_2(THF)_2]$ (**2b**), $[L_2Cr^{III}_2]$ (**3**), $[L(V^{IV}O)_2(OCHMe_2)]$ (**4**) and $[L_2(V^{V}O)_2]$ (**5**) with a pentadentate phenol-containing ligand H_3L (= $C_6H_2(CH_3)(OH)\{[C(CH_3)_3]_2(OH)NCH\}_2$) bearing the N_2O_3 donor atoms have been synthesized and the X-ray structures of **1**, **2b**, **4** and **5** are reported. The compounds were characterized by IR, UV/Vis and Mössbauer spectroscopy, mass spectrometry, electrochemical and variable-temperature (2–295 K) magnetic susceptibility measurements. Analysis of the susceptibility data demonstrates antiferromagnetic interactions between the metal centers establishing diamagnetic ground states for complexes **1**–**4**. The electrochemical results suggest the generation of ligand-centered oxidation processes attributable to the phenoxyl radicals, rather than the formation of unusually high oxidation states at the central metal centers. The ligand H_3L has the potential to act in a multidentate fashion as evidenced by the X-ray structures of **2b** and **5**. In compound **2b** the central phenolate oxygen of the *p*-cresol ring does not function as a bridging atom between two manganese centers, whereas in **5** the ligand is tetradentate with one noncoordinating nitrogen atom.

Introduction

This work stems from our ongoing interest[1] in phenol-containing ligands, and their one-electron oxidation products, i.e. phenoxyl radicals. The widespread occurrence of tyrosine radicals[2] in metalloproteins involving oxygen-dependent enzymatic radical catalysis has prompted inorganic chemists to model tyrosine by using phenolate ligands.[3] In an earlier paper[4] we described a dinucleating Schiff-base ligand H_3L, obtained by the condensation (1+2) of 2,6-diformyl-4-methylphenol with 6-amino-2,4-di-*tert*-butylphenol. This ligand can be used to prepare complexes containing Cu^{II}_2, Cu^{II}_4, Ni^{II}_2 and Ni^{II}_4 cores, which have been spectroscopically and structurally characterized and reported.[4] This paper is a continuation of our investigations with the ligand H_3L and describes coordination of the ligand with the Fe^{III}, Mn^{III}, Cr^{III}, (V^{IV}=O) and (V^{V}=O) ions. The compounds described here are given below with their labels.

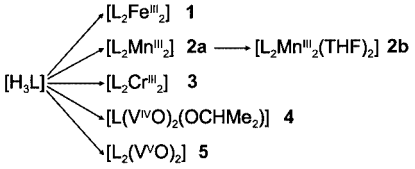

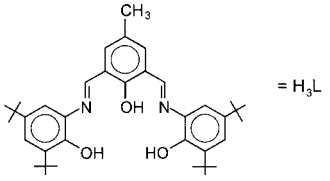

Results and Discussion

Reactions of metal salts with the ligand H_3L in the presence of triethylamine afforded complexes **1**–**5** in moderate yield. The dinuclear complexes were easily isolated and characterized by different methods. Remarkably $[L_2Mn^{II}_2]$ (**2a**), which is considered to possess an identical coordination sphere and atom connectivity as the structurally characterized $[L_2Fe^{III}_2]$ (**1**), yields on recrystallization from THF $[L_2Mn^{III}_2(THF)_2]$ (**2b**), in which the phenolate-bridging between two manganese centers prevailing in **2a** does not persist any more, thus resulting in a comparatively long Mn···Mn separation (6.45 Å).

[a] Max-Planck-Institut für Strahlenchemie,
Stiftstrasse 34–36, 45470 Mülheim an der Ruhr, Germany
E-mail: Chaudh@mpi-muelheim.mpg.de

  DOI: 10.1002/ejic.200200594

Selected IR spectroscopic data for complexes **1**−**5** are given in the Exp. Sect. The sharp peaks in the solid state FTIR spectrum due to ν(OH) of the ligand H_3L occur at 3523, 3492 and 3348 cm^{-1}. These bands are missing in **1**−**5**, indicating that on complexation the phenol-character of the ligand has been lost. There are several peaks in the region 3000−2800 cm^{-1} due to the *tert*-butyl groups along with the other ν(C−H), ν(C=C), ν(C=N) and ν(C−O) vibrations found in the normal range for these types of linkages. For **4** the sharp strong-band at 990 cm^{-1} is associated with the ν(V=O) vibration. The corresponding band for **5** occurs at 996 cm^{-1}.

The EI mass spectrum of **1** exhibits the molecular ion peak centered around *m*/*z* = 1247 with the expected isotopic distribution pattern, unambiguously indicating the composition to be Fe_2L_2. For **2a** the parent ion peak corresponds to a small peak centered around *m*/*z* = 1244; the peaks with the greatest intensities are observed at *m*/*z* = 206, 351 and 568. EI-MS unambiguously indicates the presence of THF in **2b**. Compound **3** shows the main peak at *m*/*z* = 1239 in the MS-ESI (positive) spectrum in CH_2Cl_2, indicating the composition to be Cr_2L_2, similar to that of **1**. In the EI mass spectrum of **4,** the parent ion peak with an abundance of ≈21% is observed at *m*/*z* = 760 with the expected isotopic distribution pattern. The peak at *m*/*z* = 718 with an abundance of 100% corresponding to the V_2O_3L species is also observed. In addition there are other peaks including one at *m*/*z* = 702 corresponding to the V_2O_2L species. EI-MS for **5** does not leave any doubt about the composition being $V_2O_2L_2$, with the molecular ion peak at *m*/*z* = 1268; the base peak (100%) with *m*/*z* = 1251 corresponds to V_2L_2O. The other significant peaks at *m*/*z* = 1236 and 618 are attributed to the $V_2L_2^{+}$ and $V_2L_2^{2+}$ ions.

Single Crystal X-ray Diffraction Studies

Structure of $[L_2Fe_2^{III}]\cdot 2.5CH_3CN$ (1)

Although H_3L is particularly suited to the formation of dinuclear complexes, and the analytical and spectroscopic data are in agreement with the presence of a dinuclear Fe_2L_2 unit as the smallest unit in **1**, an X-ray analysis was undertaken to remove any doubt regarding connectivity. Indeed, the structural analysis shows the presence of two six-coordinate iron(III) centers within the $Fe_2O_6N_4$ coordination unit. An ORTEP drawing of the molecule is shown in Figure 1 with selected bond lengths and angles provided in Table 1.

The iron atoms, Fe(1) and Fe(2), are in distorted octahedral environments with FeN_2O_4 coordination spheres. The two octahedra share a common edge and are bridged by two phenolate oxygen atoms O(50) and O(10). The six oxygen atoms of two ligands are roughly coplanar with the two Fe atoms. Thus, for the two iron centers, the Fe(1)O(1)O(41)O(50)O(10) and Fe(2)O(62)O(22)O(50)O(10) atoms constitute the equatorial planes. Each iron center is coordinated to two nitrogen atoms, e.g. Fe(1)−N(7) and Fe(1)−N(47), which are *trans* to each other with an angle

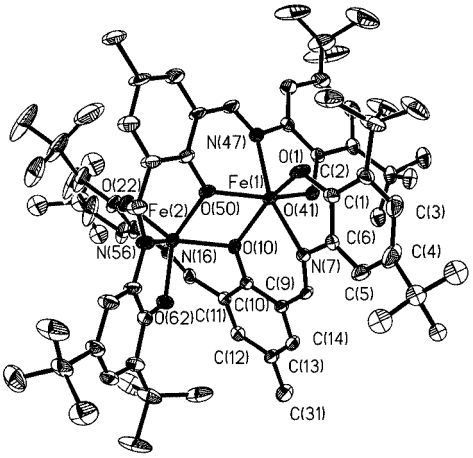

Figure 1. An ORTEP drawing of the neutral molecule $[L_2Fe_2^{III}]\cdot 2.5CH_3CN$ (**1**)

Table 1. Selected interatomic distances (Å) and angles (degrees) in $[Fe_2^{III}L_2]\cdot 2.5CH_3CN$ (**1**)

Fe(1)−O(1)	1.913(4)	Fe(1)···Fe(2)	3.32(1)
Fe(1)−O(41)	1.914(3)		
Fe(1)−O(10)	2.042(4)		
Fe(1)−O(50)	2.044(4)		
Fe(1)−N(47)	2.161(4)		
Fe(1)−N(7)	2.166(4)		
Fe(2)−O(62)	1.920(4)		
Fe(2)−O(22)	1.927(4)		
Fe(2)−O(50)	2.041(4)		
Fe(2)−O(10)	2.044(3)		
Fe(2)−N(16)	2.167(5)		
Fe(2)−N(56)	2.174(5)		
O(1)−Fe(1)−O(41)	100.2(2)	O(62)−Fe(2)−O(22)	122.5(2)
O(1)−Fe(1)−O(10)	150.9(2)	O(62)−Fe(2)−O(50)	135.4(2)
O(41)−Fe(1)−O(10)	99.8(2)	O(22)−Fe(2)−O(50)	94.3(2)
O(1)−Fe(1)−O(50)	99.9(2)	O(62)−Fe(2)−O(10)	93.4(2)
O(41)−Fe(1)−O(50)	150.8(2)	O(22)−Fe(2)−O(10)	135.9(2)
O(10)−Fe(1)−O(50)	71.1(2)	O(50)−Fe(2)−O(10)	71.2(2)
O(1)−Fe(1)−N(47)	89.6(2)	O(62)−Fe(2)−N(16)	88.8(2)
O(41)−Fe(1)−N(47)	79.1(2)	O(22)−Fe(2)−N(16)	77.2(2)
O(10)−Fe(1)−N(47)	114.9(2)	O(50)−Fe(2)−N(16)	126.3(2)
O(50)−Fe(1)−N(47)	80.0(2)	O(10)−Fe(2)−N(16)	79.1(2)
O(1)−Fe(1)−N(7)	79.2(2)	O(62)−Fe(2)−N(56)	77.6(2)
O(41)−Fe(1)−N(7)	89.9(2)	O(22)−Fe(2)−N(56)	88.9(2)
O(10)−Fe(1)−N(7)	79.9(2)	O(50)−Fe(2)−N(56)	79.1(2)
O(50)−Fe(1)−N(7)	114.6(2)	O(10)−Fe(2)−N(56)	126.3(2)
N(47)−Fe(1)−N(7)	162.7(2)	N(16)−Fe(2)−N(56)	151.3(2)

N(47)−Fe(1)−N(7) of 162.7(2)°, and which belong to two different L^{3-} ligands.

The non-bridging Fe−O bond lengths [Fe(1)−O(1), Fe(1)−O(41) av. 1.913(4) and Fe(2)−O(62), Fe(2)−O(22) av. 1.923(7) Å] are distinctly different from the bridging Fe−O bond lengths [Fe(1)−O(10), Fe(1)−O(50) av. 2.043(5) and Fe(2)−O(10), Fe(2)−O(50) av. 2.043 Å]. The symmetry in the bridging bond lengths in the nearly planar Fe_2O_2 rhomboid is noteworthy. Although the Fe−O−Fe angle of 108.9(2)° in **1** falls into the range of 105−110° observed for previously structurally characterized $Fe_2^{III}(OPh)_2$ bridges, the Fe···Fe separation of 3.32 Å is one of the longest yet found for complexes with this bis(phenox-

ide) bridge.[5−8] In the previously reported complex $[Fe_2^{III}(salmp)_2]$,[8] where salmp^{3-} is the pentadentate ligand 2-bis(salicylidenamino)methylphenolate, the Fe−O−Fe angle of 97° is the smallest yet found. Primarily because of the differences in the Fe−O−Fe angles, the magnetic properties of **1** differ considerably from those of $[Fe_2^{III}(salmp)_2]$, although **1** and $[Fe_2^{III}(salmp)_2]$ are otherwise very similar. The Fe−N and Fe−O bond lengths are consistent with a high-spin electron configuration for both Fe^{III} centers in **1** with imine nitrogen and phenolate oxygen donor ligands. The d^5 high spin electron configuration has also been confirmed both by Mössbauer spectroscopy and magnetic susceptibility measurements.

Molecular Structure of $[Mn_2^{III}L_2(THF)_2]\cdot 4CH_3CN$ (2b)

Deep orange single crystals of **2b** were obtained by slow evaporation of a tetrahydrofuran solution of **2a**. The structure of **2b** is shown in Figure 2 with selected bond lengths and angles provided in Table 2. The molecule is based on two MnO_4N_2 octahedra, in which two triply deprotonated ligands $[O^{\cap}N^{\cap}O^{\cap}N^{\cap}O]^{3-}$ span between the two manganese centers. The pentadentate ligand $[O^{\cap}N^{\cap}O^{\cap}N^{\cap}O]$ acts as a tridentate (*O*,*N*,*O*)-donor ligand to one manganese center, whilst the residual two donor atoms *N*,*O* coordinate to the second manganese center. Thus, each of the manganese centers attains only pentacoordination through the ligand. The sixth coordination site of each manganese center is occupied by the oxygen atom of a tetrahydrofuran molecule. That the manganese centers are in the +III oxidation state is evident from the axial elongation of the octahedra along the N(47)−Mn(1)−O(80) and the N(16)−Mn(2)−O(90) axes, as expected for a Jahn−Teller distorted high-spin d^4 ion. The atoms Mn(1)N(7)O(1)O(41)O(14) and Mn(2)N(56)O(54)O(22)O(62) comprise the equatorial planes for each octahedron around the Mn(1) and Mn(2) centers respectively. The $MnNO_3$ fragment is essentially planar, the maximum deviation from the mean plane being 0.01 Å. Of note is the axial position of each coordinated tetrahydrofuran molecule. The average equatorial Mn−O and Mn−N distances of 1.896(16) and 2.006(3) Å respectively, fall in the range reported for other structurally characterized d^4 Mn^{III} complexes,[9] and is also consistent with the susceptibility measurements. The smallest acute bite angle between the phenolate O atom and the N atom of the L^{3-} ligand has been found for the Mn(1) center with the angle O(41)−Mn(1)−N(47) being 77.2(1)°.

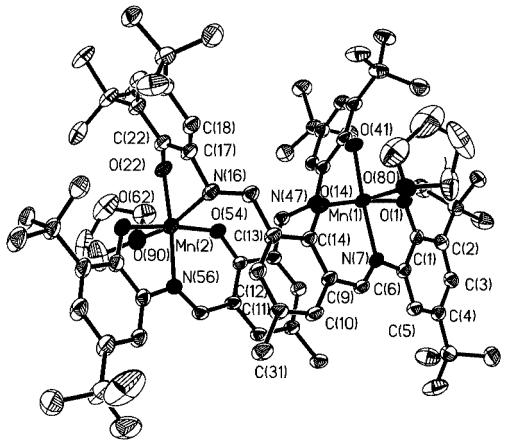

Figure 2. Molecular structure of $[L_2Mn_2^{II}(THF)_2]\cdot 4CH_3CN$ (**2b**)

Table 2. Selected bond lengths (Å) and angles (deg) for $[Mn_2^{III}L_2(THF)_2]\cdot 4CH_3CN$ (**2b**)

Mn(1)−O(1)	1.879(2)
Mn(1)−O(41)	1.899(2)
Mn(1)−O(14)	1.907(2)
Mn(1)−N(7)	2.005(2)
Mn(1)−O(80)	2.291(3)
Mn(1)−N(47)	2.310(3)
Mn(2)−O(62)	1.888(2)
Mn(2)−O(22)	1.896(2)
Mn(2)−O(54)	1.906(2)
Mn(2)−N(56)	2.008(3)
Mn(2)−O(90)	2.271(3)
Mn(2)−N(16)	2.341(3)
O(1)−Mn(1)−O(41)	89.79(9)
O(1)−Mn(1)−O(14)	174.17(9)
O(41)−Mn(1)−O(14)	95.98(9)
O(1)−Mn(1)−N(7)	82.77(10)
O(41)−Mn(1)−N(7)	172.21(10)
O(14)−Mn(1)−N(7)	91.49(10)
O(1)−Mn(1)−O(80)	94.12(10)
O(41)−Mn(1)−O(80)	94.36(10)
O(14)−Mn(1)−O(80)	84.60(10)
N(7)−Mn(1)−O(80)	88.51(10)
O(1)−Mn(1)−N(47)	92.67(10)
O(41)−Mn(1)−N(47)	77.16(10)
O(14)−Mn(1)−N(47)	89.46(10)
N(7)−Mn(1)−N(47)	100.79(10)
O(80)−Mn(1)−N(47)	169.12(9)
O(62)−Mn(2)−O(22)	90.85(10)
O(62)−Mn(2)−O(54)	173.90(10)
O(22)−Mn(2)−O(54)	95.21(9)
O(62)−Mn(2)−N(56)	82.45(10)
O(22)−Mn(2)−N(56)	173.02(10)
O(54)−Mn(2)−N(56)	91.52(10)
O(62)−Mn(2)−O(90)	93.88(10)
O(22)−Mn(2)−O(90)	88.62(10)
O(54)−Mn(2)−O(90)	85.61(10)
N(56)−Mn(2)−O(90)	93.79(11)
O(62)−Mn(2)−N(16)	91.94(10)
O(22)−Mn(2)−N(16)	76.16(10)
O(54)−Mn(2)−N(16)	90.17(10)
N(56)−Mn(2)−N(16)	101.98(11)
O(90)−Mn(2)−N(16)	163.78(10)
Mn(1)···Mn(2)	6.448(2)

Compound **2b** is a rare example of a complex bearing a dinucleating ligand containing the central *p*-cresol group,[10] in which the central phenolate oxygen, O(54) or O(14), of the cresol ring does not coordinate as a bridging atom between two metal centers.

Molecular Structure of $[L(V^{IV}{=}O)_2OCHMe_2]\cdot CH_3CN$ (4)

The structure of **4** (Figure 3) shows a divanadyl(IV) complex with a bridging isopropoxide originating from the vanadium isopropoxide starting material. The atoms V(1) and V(2) are additionally bridged by a phenolate oxygen O(10). The pentacoordination of each vanadium atom is achieved

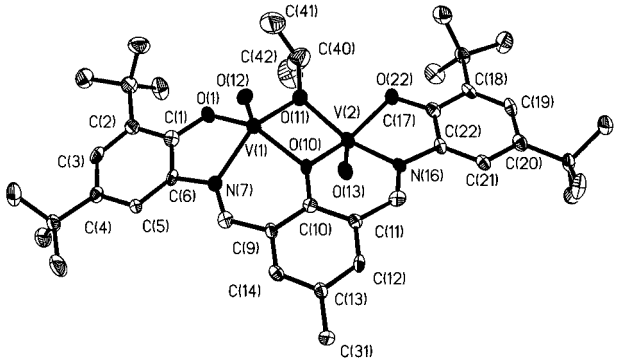

Figure 3. Molecular structure of $[L(V^{IV}{=}O)_2(OCHMe_2)]{\cdot}CH_3CN$ (**4**)

by oxygen atoms O(12) and O(13), with V(1)−O(12) and V(2)−O(13) distances of 1.586(3) and 1.588(3) Å respectively, indicating their double-bond character. The V=O groups are *trans* to each other in the di-vanadium complex. The coordination polyhedra for the vanadium centers are distorted square pyramidal with O(1)N(7)O(11)O(10) for V(1) and O(22)N(16)O(11)O(10) for V(2) forming the basal planes, in which both V(1) and V(2) are located 0.60 Å out of the equatorial planes. The ring V(1)O(11)V(2)O(10) is not planar, the dihedral angle being 10.3°. The distances V−O and V−N are in the ranges reported for comparable complexes[11] and are in agreement with the d^1 electron configuration for the vanadium centers. This electronic structure has also been confirmed by the magnetic susceptibility measurements. The separation V(1)···V(2) of 3.063 Å necessitates consideration of a direct interaction between the metal centers. Selected interatomic distances and bond angles are listed in Table 3.

Table 3. Selected bond lengths (Å) and angles (deg) for $[L(V{=}O)_2(OCHMe_2)]{\cdot}CH_3CN$ (**4**)

V(1)−O(12)	1.586(3)
V(1)−O(1)	1.905(3)
V(1)−O(11)	1.970(3)
V(1)−O(10)	1.995(3)
V(1)−N(7)	2.066(4)
V(2)−O(13)	1.588(3)
V(2)−O(22)	1.919(3)
V(2)−O(11)	1.953(3)
V(2)−O(10)	1.994(3)
V(2)−N(16)	2.065(4)
O(12)−V(1)−O(1)	109.3(2)
O(12)−V(1)−O(11)	110.6(2)
O(1)−V(1)−O(11)	95.45(13)
O(12)−V(1)−O(10)	107.86(14)
O(1)−V(1)−O(10)	142.13(14)
O(11)−V(1)−O(10)	77.92(12)
O(12)−V(1)−N(7)	102.6(2)
O(1)−V(1)−N(7)	80.16(14)
O(11)−V(1)−N(7)	146.03(14)
O(10)−V(1)−N(7)	85.12(13)
O(13)−V(2)−O(22)	107.3(2)
O(13)−V(2)−O(11)	110.9(2)
O(22)−V(2)−O(11)	94.61(13)
O(13)−V(2)−O(10)	106.1(2)
O(22)−V(2)−O(10)	146.22(13)
O(11)−V(2)−O(10)	78.36(12)
O(13)−V(2)−N(16)	105.7(2)
O(22)−V(2)−N(16)	79.87(14)
O(11)−V(2)−N(16)	142.89(14)
O(10)−V(2)−N(16)	86.15(13)
V(2)−O(10)−V(1)	100.30(13)
V(2)−O(11)−V(1)	102.65(14)
V(1)···V(2)	3.063(1)

Structure of $[L_2(VO)_2]{\cdot}2CH_3CN$ (5)

Crystals of $[L_2(VO)_2]{\cdot}2CH_3CN$, obtained by crystallizing **5** from an acetonitrile solution, were subjected to a single-crystal X-ray diffraction study at 100 K. Figure 4 shows a perspective view and the atom-labeling scheme for **5**. Selected bond parameters are listed in Table 4.

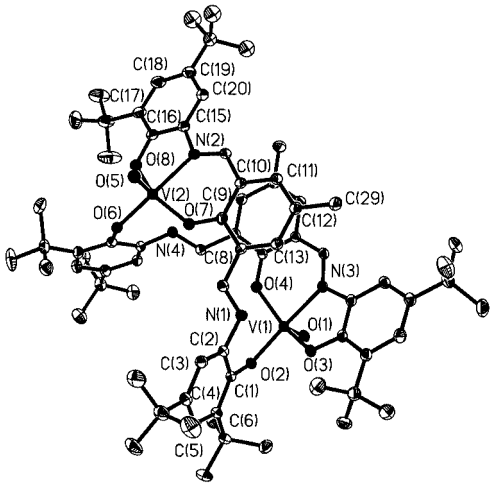

Figure 4. A perspective view of the neutral complex $[L_2(V^{V}O)_2]{\cdot}2CH_3CN$ (**5**)

In the distorted square pyramidal VO_4N coordination spheres, the metal atoms are displaced toward the O(1) or O(5) atoms from the equatorial planes O(2)O(3)N(3)O(4) for V(1) and O(6)O(7)N(2)O(8) for V(2) by 0.33 and 0.31 Å respectively. The V(1)−O(1) and V(2)−O(5) distances of 1.603(2) and 1.595(2) Å correspond to vanadium−oxygen multiple bonds and closely resemble vanadium(v) complexes containing a single V=O group.[12] Each ligand with its five donor atoms spans between two vanadium(v) centers but one N atom, N(1) or N(4), does not coordinate to any of the metal centers, making each of the ligands tetradentate. *Such behaviour for ligands based on 2,6-diformyl-p-cresol has not been observed before.* A schematic drawing of the coordination sphere is shown below to highlight the tetradentate coordination of the ligand.

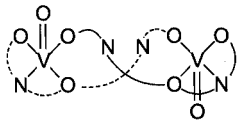

The V−O and V−N bond lengths (Table 4) are similar to those seen in vanadium(v) complexes bearing monooxo- and *cis*-dioxo-vanadium moieties.[13] The C−O (average 1.34 Å) and the aromatic C−C (average 1.40 Å) bond

Table 4. Selected bond lengths (Å) and angles (deg) for $[L_2(VO)_2]\cdot 2CH_3CN$ (**5**)

V(1)−O(1)	1.603(2)
V(1)−O(2)	1.8202(13)
V(1)−O(4)	1.8787(14)
V(1)−O(3)	1.883(2)
V(1)−N(3)	2.108(2)
V(2)−O(5)	1.595(2)
V(2)−O(6)	1.8340(14)
V(2)−O(7)	1.874(2)
V(2)−O(8)	1.875(2)
V(2)−N(2)	2.124(2)
O(1)−V(1)−O(2)	100.01(7)
O(1)−V(1)−O(4)	101.12(7)
O(2)−V(1)−O(4)	102.23(6)
O(1)−V(1)−O(3)	105.51(7)
O(2)−V(1)−O(3)	88.66(6)
O(4)−V(1)−O(3)	148.96(7)
O(1)−V(1)−N(3)	93.26(7)
O(2)−V(1)−N(3)	163.17(7)
O(4)−V(1)−N(3)	85.14(6)
O(3)−V(1)−N(3)	77.78(6)
O(5)−V(2)−O(6)	98.01(7)
O(5)−V(2)−O(7)	100.17(8)
O(6)−V(2)−O(7)	102.69(6)
O(5)−V(2)−O(8)	104.38(8)
O(6)−V(2)−O(8)	89.26(7)
O(7)−V(2)−O(8)	150.87(7)
O(5)−V(2)−N(2)	95.41(7)
O(6)−V(2)−N(2)	163.20(7)
O(7)−V(2)−N(2)	84.75(6)
O(8)−V(2)−N(2)	77.61(7)

lengths are in the expected range. The ligand is thus chelated in the trianionic phenolate form and the compound is correctly described with a formal oxidation state of +v for the vanadium ion with a d^0 electron configuration. The diamagnetism and ^{51}V NMR spectroscopic data for **5** corroborate this assignment

Mössbauer Isomer Shifts and Quadrupole Splitting

The Mössbauer spectrum of **1** at 80 K in a zero applied magnetic field and the nonlinear least-squares fit are shown in Figure 5. The spectrum was fitted with a single quadrupole split doublet with an isomer shift of $\delta = 0.518$ mm·s^{-1} and a quadrupole splitting of $\Delta E_Q = 0.754$ mm·s^{-1}. This isomer shift is consistent with those observed for high spin iron(III) ions in an octahedral or distorted octahedral environment.[14] The magnitude of the quadrupole splitting is a reflection of the unsymmetrical electric field gradient about each high-spin iron(III) site, although the two metal sites are equivalent.

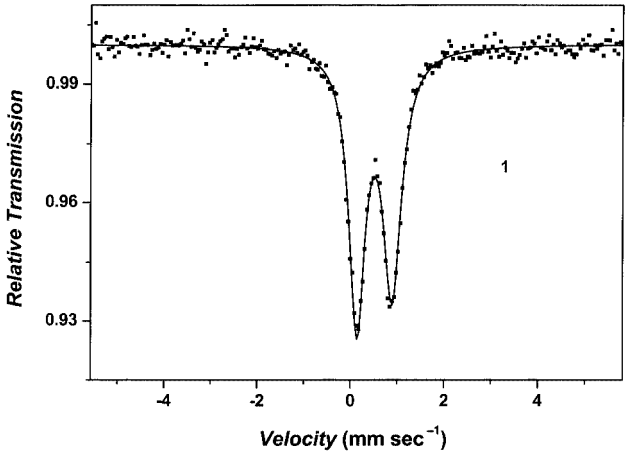

Figure 5. Mössbauer spectrum of **1** at 80 K in an applied zero-field

Magnetic Susceptibility Measurements

Variable temperature solid-state magnetic susceptibility measurements were performed on powdered samples of **1**−**4** over the temperature range 2−290 K in an applied magnetic field of 1 T (Figure 6). We used the Heisenberg spin Hamiltonian in the form $H = -2J\hat{S}_1\cdot\hat{S}_2$ for an isotropic exchange coupling between the two spins S_1 and S_2. The experimental magnetic data were simulated (shown as solid lines in Figure 6) by using a least-squares fitting computer program with a full-matrix diagonalization of exchange coupling, Zeeman splitting and axial single-ion zero-field interactions (DS_z^2), if necessary.

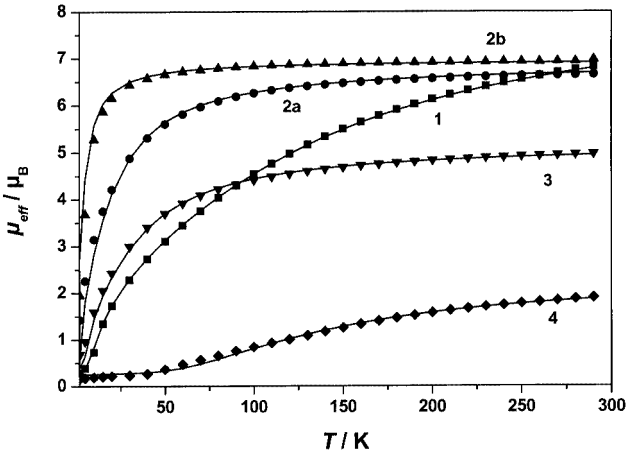

Figure 6. Plots of μ_{eff} vs. T for solid **1**−**4**. The solid lines represent the best fits of the data to the exchange coupling models

The magnetic behavior of $[Fe_2^{III}L_2]$ (**1**), is characteristic of an antiferromagnetically coupled dinuclear complex. At 290 K the μ_{eff} value of 6.784 μ_B ($\chi_M\cdot T = 5.755$ cm^3·K·mol^{-1}) decreases monotonically with decreasing temperature until it reaches a value of 0.274 μ_B ($\chi_M\cdot T = 9.380 \times 10^{-3}$ cm^3·K·mol^{-1}) at 2 K. This is a clear indication of exchange coupling between two paramagnetic Fe^{III} centers ($S_{Fe} = {}^5/_2$) with a resultant $S_t = 0$ ground state. The solid line in Figure 6 represents the best fit with the following parameters: $J = -12.7$ cm^{-1}, $g = 2.00$ (fixed) and PI ($S = {}^5/_2$) = 0.003. The calculated antiparallel exchange is in keeping with the range observed for comparable diphenoxo-bridged ferric dimers.[1,6,7]

Two semi-empirical magnetostructural correlations relating the magnitude of the exchange coupling to the iron-

oxygen bond length in exchange coupled phenoxo-, alkoxo- and hydroxo-bridged dinuclear iron(III) compounds have been proposed.[5,7] By using the empirical relationship $J = -10^7 \exp(-6.8d)$,[7] where d is the averaged iron−oxygen distance, 2.043 Å for **1**, the J value for **1** can be calculated to be -9.25 cm^{-1}, which differs from the experimentally observed value of -12.7 cm^{-1}. The second equation[5] leads to a calculated value of -5.1 cm^{-1}. Regrettably, none of these two correlations can satisfactorily reproduce the exchange interaction in **1**.

The magnetic moment, μ_{eff}/molecule, for $[L_2Mn_2^{III}]$ (**2a**) of 6.636 μ_B ($\chi_M{\cdot}T$ = 5.507 cm$^3{\cdot}$K$\cdot$mol^{-1}) at 290 K decreases monotonically with decreasing temperature until it reaches a value of 1.421 μ_B ($\chi_M{\cdot}T$ = 0.2523 cm$^3{\cdot}$K$\cdot$mol^{-1}) at 2 K. This temperature dependence of μ_{eff} is a clear indication of an antiferromagnetic exchange coupling between two paramagnetic Mn^{III} (S_{Mn} = 2) centers. A least-squares fit, shown as the solid line in Figure 6, with $J = -2.95$ cm^{-1} and g = 1.98 was obtained. Thus a weak exchange coupling is operating between the Mn^{III} centers through the diphenoxo-bridge and, as expected, the exchange interaction is weaker in **2a** than that in **1**. The exchange coupling operating in **2b** is even weaker than that in **2a**, as evidenced from the temperature-dependence of μ_{eff} for **2b**. The magnetic moment μ_{eff} varies only slightly (μ_{eff} = 6.94 to 6.54 μ_B) in the temperature range 290−40 K, but then starts to decrease monotonically reaching a value of 1.94 μ_B at 2 K. Simulation of the experimental magnetic data yields $J = -0.66$ cm^{-1} and g = 1.995 (the solid line in Figure 6). The antiferromagnetic coupling in **2b** which is weaker than in **2a** is in agreement with the dimeric solid state structure of **2b** in which the manganese(III) centers are 6.45 Å apart.

The experimental magnetic moment of **3** decreases from 4.95 μ_B ($\chi_M{\cdot}T$ = 3.064 cm$^3{\cdot}$K$\cdot$mol^{-1}) at 290 K to an essentially diamagnetic value of μ_{eff} = 0.677 μ_B ($\chi_M{\cdot}T$ = 0.05736 cm$^3{\cdot}$K$\cdot$mol^{-1}) at 2 K, resulting from the antiferromagnetic interaction between the two Cr^{III} ions bridged by a diphenoxo group. The solid line in Figure 6 represents the best fit with the following parameters: $J = -7.6$ cm^{-1}, g = 1.893 and PI (S = $^3/_2$) = 0.01. The calculated antiparallel exchange falls in the range observed for comparable phenoxo-alkoxo-bridged chromium(III) dimers.[15−16]

The temperature dependence of the molar magnetic susceptibility χ_M for **4** shows a clear maximum around 230 K, consistent with the presence of significant antiferromagnetic coupling. Increases in χ_M at low temperatures ($\leq$ 30 K) have often been seen in strongly antiferromagnetically coupled systems and arise from a small amount of paramagnetic impurity in the sample. The magnetic moment of **4** is 1.83 μ_B ($\chi_M{\cdot}T$ = 0.4197 cm$^3{\cdot}$K$\cdot$mol^{-1}) at 290 K, which is significantly lower than the spin-only value of 2.45 μ_B for two uncoupled S = $^1/_2$ spins. Furthermore μ_{eff} gradually decreases on decreasing the temperature, reaching 0.15 μ_B at 2 K. The data were fitted using the following parameters: $J = -128.5$ cm^{-1}, g = 1.90, PI (S = $^1/_2$) = 0.018, TIP = 80 $\times 10^{-6}$ cm$^3{\cdot}$mol^{-1} and $\theta = -3.0$ K. The antiferromagnetic coupling constant of -128.5 cm^{-1} lies in the range of values found for other dinuclear vanadyl(IV) complexes[11,17] containing phenoxo, alkoxo and hydroxo-bridging ligands.

^{51}V NMR Measurements

Compound **5** containing V^V with a d^0 electron configuration is diamagnetic and was examined by ^{51}V NMR spectroscopy[18] with $VOCl_3$ in C_6D_6 as an internal standard. The compound gives rise to a single signal at $\delta = -420$ ppm, suggesting that there is only one species in solution, as in the solid state (vide infra).

Electrochemistry and Spectroelectrochemistry

The electrochemical properties of complexes **1** (Fe^{III}), **2a** (Mn^{III}) and **3** (Cr^{III}) were investigated in CH_2Cl_2 solutions containing 0.1 M TBA(PF_6). Voltammetric experiments (cyclic voltammetry, CV and square wave voltammetry, SQW) reveal that all three compounds can undergo three consecutive oxidations.

Figure 7 shows representative examples of the electrochemical measurements. The respective redox potentials vs. the Fc^+/Fc couple are compiled in Table 5. The first two oxidations are reversible on the time scale of cyclic voltammetry (scan rates 0.05−0.5 V/s). The peak positions are almost independent of the scan rates and the peak separations are close to the values observed for ferrocene under the same conditions (0.08 V). The third oxidations are

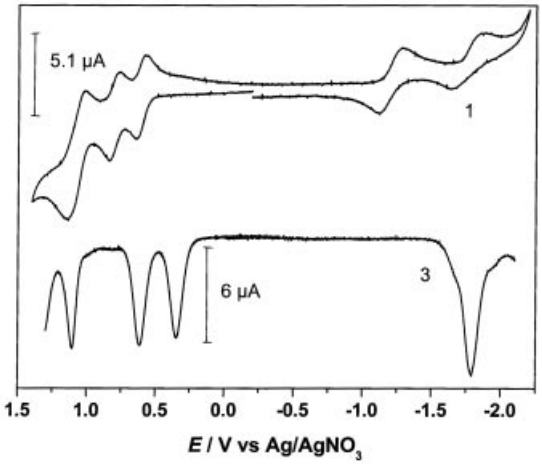

Figure 7. Cyclic voltammogram (50 mV/s) of **1** (top) and square wave voltammogram at 25 Hz of **3** (bottom) in CH_2Cl_2 [0.1 M nBu$_4$NPF$_6$]

Table 5. Redox potentials ($E_{1/2}$ in Volt vs. Fc^+/Fc) for reduction and oxidation of complexes **1−3**

	$E_{1/2}$ (ox3)[a][b]	$E_{1/2}$ (ox2)	$E_{1/2}$ (ox1)	$E_{1/2}$ (red1)	$E_{1/2}$ (red2)
1 (Fe^{III})	+0.870	+0.586	+0.390	−1.42	−1.95
2a (Mn^{III})	+0.860[c]	+0.542	−0.060	−1.30	
3 (Cr^{III})	+0.905[c]	+0.410	+0.144	−1.99[c]	

[a] CV and SQW in CH_2Cl_2 solutions containing 0.1 M nBu$_4$NPF$_6$; working electrode: 2-mm glassy carbon disk. [b] Fc^+/Fc in CH_2Cl_2 vs. Ag/AgNO$_3$: $E_{1/2}$ = 0.216 V for **1**, 0.240 V for **2b** and 0.203 V for **3**. [c] Chemically irreversible; square wave peak potentials are given.

either chemically irreversible (**2a** and **3**; no reverse peaks observable) or contain an irreversible component (**1**; oxidation peak at all scan rates twice as high as the peak of re-reduction and of the reversible peaks).

The redox potentials of the second and third oxidations are very similar for all three compounds irrespective of the nature of the central metal ion. This provides firm evidence that these oxidations are ligand centered and give rise to phenoxyl radicals.

The redox potentials of the first oxidations are spread over a somewhat larger range (Table 5). In particular, the redox potential of **2a** is low and could be due to formation of the Mn^{IV} oxidation state. We therefore performed spectroelectrochemical measurements at −25 °C and found that the spectral changes upon the first oxidation of **2a** show the fingerprints for phenoxyl radical formation.[19] In the difference spectra a new peak with a maximum at 417 nm developed together with a broad band which extends from 650−950 nm and has a maximum at ≈800 nm. Therefore, the first oxidation of **2a** can be clearly assigned to phenoxyl radical formation. In spectroelectrochemical experiments with **1** and **3**, an increase in absorption at 350−450 nm and at >700 nm was observed during the first oxidation, as expected for formation of phenoxyl radicals. However, the maxima of the difference spectra were at 350−370 nm rather than at 400−420 nm. It is most likely that these spectra are distorted by small oxidation-induced shifts in the very intense charge-transfer bands of the complexes (the ε-values of the starting material are ten times higher than those of phenoxyl radicals at the respective wavelengths). In view of the similarity of the redox potentials of **1** and **3** we therefore conclude that in these complexes the first oxidations also represent formation of phenoxyl radicals.

The reductions at potentials of less than −1 V are either electrochemically quasi-reversible (**1** and **2a**; peak separation 0.15−0.25 V at 0.2 V/s scan rate) or chemically irreversible (**3**; high peak current and lack of reverse peak). They were not further investigated and are most likely metal-centered reductions to the M^{2+} oxidation states.

A few experiments were done with the Vanadium V^V compound $[L_2(V{=}O)_2]$ (**5**). The square wave voltammogram exhibits three oxidations in the accessible potential range, two reversible ones at −0.136 V and +0.226 V and one irreversible at +1.02 V. These oxidations, which occur in the same potential range as those of **1**−**3**, we also tentatively assign to phenoxyl radical formation. Reductions also occur in the potential range −0.7 to −0.9 V and these are most likely to be metal-centered reductions to the V^{IV} oxidation state. The square wave voltammogram, however, exhibits complex multiple peak formations and therefore accurate redox potentials cannot be evaluated.

Concluding Remarks

The structural analysis of a series of transition metal complexes derived from the pentadentate ligand H_3L demonstrates the ability of this dinucleating ligand to form complexes of metal ions of the first transition series mostly in a six-coordinate fashion. As evidenced by the square-pyramidal five-coordinate V^{IV} **4** and V^V **5** complexes, this may be overcome by electronic factors, e.g. the Jahn−Teller effect and absence of LFSE. The fact that this ligand can adapt itself to various metal ion sizes to yield dinuclear complexes makes it a versatile building block for the construction of bimetallic complexes, which might be useful for the study of biologically relevant dinuclear complexes.

From the X-ray data above and particularly those of **2b** and **5**, it is clear that within a family of complexes it is possible to obtain a variety of coordination environments. Complexes of Schiff base ligands have been in the literature for over 150 years and rigid chelating environments for the metals have been proposed for complexes of this type. The present ligand H_3L, also a Schiff-base ligand, demonstrates how the local environment around the metal becomes distorted to accommodate the increasing internal chelate ring and how the ligand itself adjusts from originally pentadentate to tetradentate in a complex. The realization that the present ligand H_3L has the potential to switch between different chelating modes highlights the prospect of designing a generic ligand system which should have a rich, interesting and independent chemistry worthy of greater exploration. Overall this Robson-type ligand with *tert*-butyl substituents has offered a new chelating flexibility.

The electrochemical results suggest the generation of ligand-centered oxidation processes attributable to the phenoxyl radicals, rather than the formation of unusually high oxidation states at the central metal centers.

Experimental Section

Materials and Physical Measurements: Reagent or analytical grade materials were obtained from commercial suppliers and used without further purification, except those for electrochemical measurements. Elemental analyses (C,H,N) were performed by the Microanalytical Laboratory Dornis & Kolbe, Mülheim, Germany. Fourier transform infrared spectra in KBr discs were recorded on a Perkin−Elmer 2000 FT-IR instrument. Electronic absorption spectra in solution were measured on a Perkin−Elmer Lambda 19 spectrophotometer. Magnetic susceptibilities of powdered samples were recorded on a SQUID magnetometer in the temperature range 2−295 K with an applied field of 1 T. Experimental susceptibility data were corrected for the underlying diamagnetism using Pascal's constants and for the TIP contributions. Cyclic voltammetric and coulometric measurements were performed on EG&G equipment (potentiostat/galvanostat model 273A). Mass spectra were recorded with either a Finnigan MAT 8200 (electron ionization, EIMS) or a MAT 95 (electrospray ESI-MS) instrument. A Bruker DRX 400 instrument was used for NMR spectroscopy.

Preparations

H_3L: The ligand H_3L was prepared as described earlier.[4]

$[L_2Fe_2^{II}]$ (1): To a degassed solution of the ligand H_3L (0.29 g; 0.5 mmol) and NEt_3 (0.12 mL) in an acetonitrile/dichloromethane solvent mixture (10 ml:15 mL) was added $Fe(ClO_4)_2{\cdot}6H_2O$ (0.18 g; 1 mmol) and the resultant solution was heated to reflux for 0.5 h under argon, then cooled and stirred in air for an hour. The result-

ant deep reddish-brown solution was kept at ambient temperature for crystallization. After 2 d red-brown microcrystals were collected by filtration and air-drying. Yield: 0.14 g (45%). $C_{74}H_{94}Fe_2O_6N_4$: calcd. C 71.26, H 7.60, Fe 8.95, N 4.49; found C 71.3, H 7.6, Fe 9.0, N 4.5. EI-MS: *m*/*z* = 1247 [M^+]. IR (KBr disk): $\tilde{\nu}$ =2953 s cm^{-1}, 2865 m, 1610 m, 1591 m, 1565 m, 1471 s, 1443 s, 1408 m, 1255 s, 1163 m, 834 m, 537 m, 492 m. UV/Vis (CH_2Cl_2): λ_{max} ($\varepsilon/M^{-1}\cdot cm^{-1}$) = 560 sh (≈7800), 421 nm (34200).

X-ray quality crystals of **1**·2.5CH_3CN were grown from an acetonitrile solution.

[$L_2Mn_2^{III}$] (2a): A methanolic solution (25 mL) of the ligand H_3L (0.29 g; 0.5 mmol), manganese(III) acetate (0.13 g; 0.2 mmol) and tetrabutylammonium methoxide (0.2 mL) was heated to reflux for 1 h. Red-brown microcrystals of **2a** were formed on cooling to room temperature. The solid was collected by filtration and air-dried. Yield: 70 mg (≈23%). $C_{74}H_{94}Mn_2N_4O_6$: calcd. C 71.36, H 7.61, Mn 8.82, N 4.50; found C 71.50, H 7.5, Mn 8.7, N 4.5. EI-MS: *m*/*z* = 1242−1246 [M^+]. IR (KBr disk): $\tilde{\nu}$ =2953 s cm^{-1}, 2866 m, 1610 m, 1587 m, 1472 m, 1442 m, 1406 m, 1360 m, 1246 s, 1161 m, 836 m, 561 m, 537 m. UV/Vis (CH_2Cl_2): λ_{max} ($\varepsilon/M^{-1}\cdot cm^{-1}$) = 470 nm (22000).

[$L_2Mn_2^{III}(THF)_2$] (2b): X-ray quality crystals of **2b**·4CH_3CN were obtained by crystallizing **2a** from a tetrahydrofuran/acetonitrile solution. $C_{82}H_{110}Mn_2N_4O_8$·4CH_3CN: calcd. C 69.57, H 7.91, Mn 7.07, N 7.21; found C 69.7, H 7.9, Mn 7.3, N 6.7.

[$L_2Cr_2^{III}$] (3): A solution of the ligand (0.29 g; 0.5 mmol), NEt_3 (0.1 mL) and $CrCl_2$ (0.12 g; 0.5 mmol) in tetrahydrofuran (25 mL) was heated to reflux under argon for 15 min and then in air for a further 1 h. The resultant deep-red solution was filtered and the filtrate was evaporated to dryness using a rotary evaporator. The solid obtained was dissolved in of THF (5 mL) and the solution was filtered to remove any solid. After addition of acetonitrile (2 mL) to the filtrate, slow evaporation at room temperature yielded **3** as an orange-red microcrystalline solid. Yield: 0.13 g (42%). $C_{74}H_{94}Cr_2N_4O_6$: calcd. C 71.70, H 7.64, Cr 8.39, N 4.52; found C 71.4, H 7.6, Cr 8.3, N 4.5. EI-MS (pos., CH_2Cl_2): *m*/*z* = 1239−1246 [M^+]. IR (KBr disk): $\tilde{\nu}$ = 2953 s cm^{-1}, 2905 m, 2867 m, 1598 m, 1565 m, 1474 s, 1445 s, 1406 m, 1256 s, 1162 m, 832 m, 569 m, 539 m, 517 m. UV/Vis (CH_2Cl_2): λ_{max} ($\varepsilon/M^{-1}\cdot cm^{-1}$) = 458 (16450), 337 sh nm (≈16000).

[$L(V^{IV}{=}O)_2\mu$-$OCH(CH_3)_2$] (4): A solution of the ligand H_3L (0.29 g; 0.5 mmol), vanadyltris(isopropoxide) (0.25 ml; 1 mmol) and Et_3N (0.3 mL) in a deoxygenated acetonitrile/dichloromethane solvent mixture (10 ml:10 mL) was heated to reflux under argon for 1 h and then stirred in air for a further 1 h. The solution was filtered to remove any solid particles and the filtrate was allowed to evaporate slowly at ambient temperature to provide deep red crystals. Yield: 0.18 g (47%). $C_{40}H_{54}N_2O_6V_2$: calcd. C 63.15, H 7.15, N 3.68, V 13.39; found C 63.1, H 7.1, N 3.6, V 13.5. EI-MS: *m*/*z* = 760 (20.8%) [M^+], 718 (100%) [$M^+ - C_3H_7$], 703 (54%) [$M^+ - C_3H_7O$]. IR (KBr disk): $\tilde{\nu}$ = 2953 s cm^{-1}, 2867 m, 1614 m, 1569 m, 1476 s, 1446 m, 1362 m, 1250 s, 1161 s, 990 vs, 948 m, 831 s, 567 m, 546 s. UV/Vis (CH_2Cl_2): λ_{max} ($\varepsilon/M^{-1}\cdot cm^{-1}$) = 363 (14900), 470 nm (10500).

X-ray quality crystals of **4**·CH_3CN were obtained by recrystallization of **4** from acetonitrile.

Table 6. Crystallographic data for [$L_2Fe_2^{III}$]·2.5 CH_3CN (**1**), [$L_2Mn_2^{II}(THF)_2$]·4 CH_3CN (**2b**), [$L(VO^{IV})_2(OCHMe_2)$]·CH_3CN (**4**) and [$L_2(VO^{V})_2$]·2 CH_3CN (**5**)

	1	**2b**	**4**	**5**
Empirical formula	$C_{74}H_{94}Fe_2N_4O_6$·2.5CH_3CN	$C_{82}H_{110}Mn_2N_4O_8$·4CH_3CN	$C_{42}H_{59}N_3O_6V_2$	$C_{74}H_{94}N_4O_8V_2$·2CH_3CN
Formula mass	1349.87	1553.84	803.80	1351.52
Temperature	100(2) K	100(2) K	100(2) K	100(2) K
Wavelength (Mo-K_α)	0.71073 Å	0.71073 Å	0.71073 Å	0.71073 Å
Crystal system	Triclinic	Triclinic	Triclinic	Triclinic
Space group	$P\bar{1}$	$P\bar{1}$	$P\bar{1}$	$P\bar{1}$
Unit cell dimensions	*a* = 16.887(2) Å	*a* = 11.6088(8) Å	*a* = 8.456(1) Å	*a* = 14.8895(8) Å
	b = 17.026(2) Å	*b* = 12.6390(8) Å	*b* = 16.087(2) Å	*b* = 16.047(1) Å
	c = 17.040(2) Å	*c* = 31.802(2) Å	*c* = 16.685(2) Å	*c* = 16.881(1) Å
	α = 115.63(2)°	α = 79.41(1)°	α = 71.35(2)°	α = 77.47(1)°
	β = 113.09(2)°	β = 83.17(1)°	β = 89.26(2)°	β = 79.50(1)°
	γ = 90.69(2)°	γ = 72.87(1)°	γ = 79.26(2)°	γ = 81.47(1)°
Volume (Å^3); *Z*	3964.7(8); 2	4372.7(5); 2	2110.2(4); 2	3846.5(4); 2
Density (calcd.) Mgm^{-3}	1.131	1.180	1.265	1.167
Absorp. coeff. (mm^{-1})	0.417	0.346	0.490	0.298
F(000)	1442	1664	852	1440
Crystal size (mm)	0.39 × 0.37 × 0.34	0.44 × 0.36 × 0.24	0.33 × 0.14 × 0.09	0.35 × 0.11 × 0.10
θ range for data collect.	1.69 to 26.00°	2.31 to 27.11°	2.16 to 22.50°	4.21 to 32.50°
Reflections collected	26505	31923	13369	44652
Independent reflect.	13350 [*R*(int.) = 0.0419]	18622 [*R*(int.) = 0.0482]	5434 [*R*(int.) = 0.0852]	27516 [*R*(int.) = 0.0452]
Absorpt. correction	SADABS	Gaussian, face indexed	Gaussian, face indexed	Gaussian, face indexed
Data/restraints/param.	13308/36/805	18622/6/1000	5430/0/479	27259/34/839
Goodness-of-fit on F^2	1.057	1.065	1.012	1.014
Final *R* indices	*R*1 = 0.0862,	*R*1 = 0.0747,	*R*1 = 0.0527,	*R*1 = 0.0681,
[$I > 2\sigma(I)$]	*wR*2 = 0.2532	*wR*2 = 0.1899	*wR*2 = 0.1194	*wR*2 = 0.1539
R indices (all data)	*R*1 = 0.1223,	*R*1 = 0.0933,	*R*1 = 0.0963,	*R*1 = 0.1102,
	*wR*2 = 0.2875	*wR*2 = 0.2020	*wR*2 = 0.1345	*wR*2 = 0.1814

$[L_2(V^V{=}O)_2]$ (5): A deoxygenated solution of the ligand (0.29 g; 0.5 mmol) and Et_3N (0.25 mL) in a solvent mixture of acetonitrile/dichloromethane (30 ml:10 mL) was charged with $V(THF)_3Cl_3$ (0.19 g; 0.5 mmol) and the resultant solution was heated to reflux under argon for 1 h and then stirred in air for a further 1 h. The clear solution was kept at room temperature for slow evaporation of the solvents. After 3 d the dark-brown crystals were collected by filtration. Yield: 0.2 g (63%). $C_{74}H_{94}N_4O_8V_2$: calcd. C 70.01, H 7.46, N 4.41, V 7.99; found C 69.83, H 7.35, N 4.40, V 7.95. EI-MS: m/z = 1266−1269 [M^+], 1251−1254 [$M^+ - CH_3$], 618 [LV^+]. IR (KBr disk): $\tilde{\nu}$ = 3442 m cm^{-1}, 2954 s, 2904 s, 2867 s, 1616 m, 1591 m, 1544 s, 1476 s, 1443 s, 1361 s, 1244 s, 996 s, 838 m. UV/Vis (CH_2Cl_2): λ_{max} (ε/M^{-1}·cm^{-1}) = ca. 414 sh (≈25600), 659 nm (5200). ^{51}V NMR: δ = −420 ppm.

X-ray quality crystals of **5**·$2CH_3CN$ were obtained from an acetonitrile solution of **5**.

X-ray Crystallographic Data Collection and Refinement of the Structures: Single crystals of **1** (orange-red), **2b** (red), **4** (orange-red) and **5** (orange-red) were coated with perfluoropolyether, picked up with glass fibers and mounted on a Kappa-CCD diffractometer equipped with a nitrogen cold stream at 100 K. Graphite-monochromated Mo-K_α radiation (λ = 0.71073 Å) was used. Crystallographic data of the compounds are listed in Table 6. Cell constants were obtained from a least-squares fit of the diffraction angles of several thousand strong reflections. Intensity data were corrected for Lorentz and polarization effects. The Siemens ShelXTL software package (G. M. Sheldrick, Universität Göttingen) was used for solution, refinement, and artwork of the structures, and the neutral atom scattering factors of the program were used. All structures were solved and refined by direct methods and difference Fourier techniques. Non-hydrogen atoms were refined anisotropically, and hydrogen atoms were placed at calculated positions and refined as riding atoms with isotropic displacement parameters.

CCDC-195241 (**1**), -195242 (**2b**), -195243 (**4**)and -195244 (**5**) contain the supplementary crystallographic data for this paper. These data can be obtained free of charge at www.ccdc.cam.ac.uk/conts/retrieving.html [or from the Cambridge Crystallographic Data Centre, 12, Union Road, Cambridge CB2 1EZ, UK; Fax: (internat.) +44-1223/336-033; E-mail: deposit@ccdc.cam.ac.uk].

Acknowledgments

Financial support from the DFG (Grant: Priority Program Ch111/2−1), the Max-Planck Society and Fonds der Chemischen Industrie is gratefully acknowledged. Thanks are due to Mrs. H. Schucht, Mrs. P. Höfer, Mr. A. Göbels, Mr. B. Mienert for skilful technical assistance.

[1] See for example: T. Weyhermüller, T. K. Paine, E. Bothe, E. Bill, P. Chaudhuri, *Inorg. Chim. Acta* **2002**, *337*, 344.

[2] *Chem. Rev.* **1996**, *96; Metal Ions in Biological Systems*, (Eds.: H. Sigel, A. Sigel, Marcel-Dekker), New York, **1994**, vol. 30; G. T. Babcock, M. Espe, C. Hoganson, N. Lydakis-Simantiris, J. McCracken, W. Shi, S. Styring, C. Tommas, K. Warncke, *Acta Chem. Scand.* **1997**, *51*, 533; M. M. Fontecave, J. L. Pierre, *Bull. Soc. Chim. Fr.* **1996**, *133*, 653; D. P. Goldberg, S. J. Lippard, *Adv. Chem. Ser.,* **1995**, *246*, 59; J. Stubbe, W. A. van der Donk, *Chem. Rev.* **1998**, *98*, 705.

[3] For example: J. A. Halfen, B. A. Jazdzewski, S. Mahapatra, L. M. Berreau, E. C. Wilkinson, L. Que, Jr, W. B. Tolman, *J. Am. Chem. Soc.* **1997**, *119*, 8217; Y. Wang, T. D. P. Stack, *J. Am. Chem. Soc.* **1996**, *118*, 13097; D. Zurita, I. Gautier-Luneau, S. Menage, J. L. Pierre, E. Saint-Aman, *J. Biol. Inorg. Chem.* **1997**, *2*, 46; E. Bill, J. Müller, T. Weyhermüller, K. Wieghardt, *Inorg. Chem.* **1999**, *38*, 5795 and references therein; M. A. Halcrow, L. M. Lindy Chia, X. Liu, E. J. L. McInnes, L. J. Yellowlees, F. E. Mabbs, I. J. Scowen, M. McPartlin, J. E. Davies, *J. Chem. Soc., Dalton Trans.* **1999**, 1753; S. Itoh, S. Takayama, R. Arakawa, A. Furuta, M. Komatsu, A. Ishida, S. Takamuku, S. Fukuzumi, *Inorg. Chem.* **1997**, *36*, 1407; K. Yamato, T. Inada, M. Doe, A. Ichimura, T. Takui, Y. Kojima, T. Kikunaga, S. Nakamura, N. Yanagihara, T. Onaka, S. Yano, *Bull. Chem. Soc. Jpn.* **2000**, *73*, 903; Y. Shimazaki, S. Huth, A. Odani, O. Yamauchi, *Angew. Chem. Int. Ed. Engl.* **2000**, *112*, 1666; M. Vaidyanathan, M. Palaniandavar, *Proc. Indian Acad. Sci. (Chem. Sci)*, **2000**, *112*, 223; C. N. Verani, E. Bothe, D. Burdinski, T. Weyhermüller, U. Flörke, P. Chaudhuri, *Eur. J. Inorg. Chem.* **2001**, 2161.

[4] S. Mukherjee, T. Weyhermüller, E. Bothe, K. Wieghardt, P. Chaudhuri, *Eur. J. Inorg. Chem.* **2003**, *5*, 863.

[5] S. M. Gorun, S. J. Lippard, *Inorg. Chem.* **1991**, *30*, 1625.

[6] A. Elmali, Y. Elerman, I. Svoboda, *Z. Naturforsch., Teil B* **2001**, *56*, 897.

[7] R. Werner, S. Ostrovsky, K. Griesar, W. Haase, *Inorg. Chim. Acta* **2001**, *326*, 78 and references therein.

[8] B. Snyder, G. S. Patterson, A. J. Abrahamson, R. H. Holm, *J. Am. Chem. Soc.* **1989**, *111*, 5214 and references therein.

[9] For example: S. B. Yu, C. P. Wang, E. P. Day, R. H. Holm, *Inorg. Chem.* **1991**, *30*, 4067.

[10] H. Okawa, H. Furutachi, D. E. Fenton, *Coord. Chem. Rev.* **1998**, *174*, 51 and references cited therein.

[11] For example: C. J. Carrano, C. M. Nunn, R. Quan, J. A. Bonadies, V. L. Pecoraro, *Inorg. Chem.* **1990**, *29*, 944; S. L. Castro, M. E. Cass, F. J. Holländer, S. L. Bartley, *Inorg. Chem.* **1995**, *34*, 466; S. Burojevic, I. Shweky, A. Bino, D. A. Summers, R. C. Thompson, *Inorg. Chim. Acta* **1996**, *251*, 75; W. Plass, *Z. Anorg. Allg. Chem.* **1997**, *623*, 1290; Y. Sun, M. Melchior, D. A. Summers, R. C. Thompson, S. J. Rettig, C. Orvig, *Inorg. Chem.* **1988**, *37*, 3119; A. S. Cecato, A. Neves, M. A. de Brito, S. M. Drechsel, A. S. Mangrich, R. Werner, W. Haase, A. J. Bortoluzzi, *J. Chem. Soc., Dalton Trans.* **2000**, 1573.

[12] Selected examples: D. C. Crans, H. Chen, O. P. Anderson, M. M. Miller, *J. Am. Chem. Soc.* **1993**, *115*, 6769; M. Bashipoor, H. Schmidt, C. Schutzke, D. Rehder, *Chem. Ber.* **1997**, *130*, 651; M. Moon, M. Pyo, Y. C. Myoung, C. I. Ahn, M. S. Lah, *Inorg. Chem.* **2001**, *40*, 554; M. S. Palacios, M. J. Rocio, S. Dominguez, P. Gill, C. Ruiz-Perez, F. V. Rodriguez-Romero, J. M. Dance, *Polyhedron* **1997**, *16*, 1143; W. Plass, *Z. Anorg. Allg. Chem.* **1997**, *623*, 461; B. Baruah, S. Das, A. Chakravorty, *Inorg. Chem.* **2002**, *41*, 4502.

[13] C. R. Cornman, G. J. Colpas, J. D. Hoeschele, J. Kampf, V. L. Pecoraro, *J. Am. Chem. Soc.* **1992**, *114*, 9925; A. Neves, W. Walz, K. Wieghardt, B. Nuber, J. Weiss, *Inorg. Chem.* **1988**, *27*, 2484.

[14] P. Gütlich, "*Mössbauer Spectroscopy*", (Ed. U. Gonser), Springer-Verlag, Berlin, Heidelberg, New York, **1975**; N. N. Greenwood, T. C. Gibb, "*Mössbauer Spectroscopy*", Chapman and Hall, London, **1971**.

[15] E. D. Estes, R. P. Scaringe, W. E. Hatfield, D. J. Hodgson, *Inorg. Chem.* **1976**, *15*, 1179; H. R. Fischer, D. J. Hodgson, E. Pedersen, *Inorg. Chem.* **1984**, *23*, 4755; A. Bencini, M. D. Vaira, F. Manni, *J. Chem. Soc., Dalton Trans.* **1991**, 41; M. Nakahanda, T. Fujihara, A. Fuyuhiro, S. Kaizaki, *Inorg. Chem.* **1992**, *31*, 1316; A. Böttcher, H. Elias, J. Gleurup, M. Neuburg, C. E. Olsen, J. Springborg, H. Weihe, M. Zehnder, *Acta Chem. Scand.,* 1994, **48**, 981; M. Ardon, A. Bino, K. Michelsen, E. Pedersen, *J. Am. Chem. Soc.* **1987**, *109*, 5855; U. Bossek, K.

Wieghardt, B. Nuber, J. Weiss, *Angew. Chem. Int. Ed. Engl.* **1990**, *29*, 1055; N. Arulsamy, J. Gleurup, D. J. Hodgson, *Inorg. Chem.* **1994**, *23*, 2066.
[16] T. K. Paine, T. Weyhermüller, K. Wieghardt, P. Chaudhuri, *Inorg. Chem.* **2002**, *41*, 6538.
[17] A. P. Ginsberg, E. Koubeck, H. J. Williams, *Inorg. Chem.* **1966**, *5*, 1656; E. F. Hasty, T. J. Colburn, D. N. Hendrickson, *Inorg. Chem.* **1973**, *12*, 2414; K. Wieghardt, U. Bossek, K. Volckmar, W. Swiridoff, J. Weiss, *Inorg. Chem.* **1984**, *23*, 1387; E. Solari, A. Klose, C. Floriani, N. Re, A. Chiesi-Villa, C. Rizzoli, *Polyhedron* **1996**, *15*, 4103; N. S. Dean, M. R. Bond, C. J. O′Connor, C. J. Carrano, *Inorg. Chem.* **1996**, *35*, 7643.
[18] D. Rehder, *Angew. Chem. Int. Ed. Engl.* **1991**, *30*, 148.
[19] C. N. Verani, E. Bothe, D. Burdinski, T. Weyhermüller, U. Flörke, P. Chaudhuri, *Eur. J. Inorg. Chem.* **2001**, 2161.

Received October 24, 2002

